INFLUENCE OF STRAIN RATE ON THE ASHBY-GIBSON PARAMETERS OF SHEET DIAMOND LATTICE STRUCTURES

Ramon Miralbes-Buil1, Natalia Santamaria-Hoyos1, Nuno Curado-Correia2, David Ranz-Angulo1

1 UNIVERSIDAD DE ZARAGOZA. EINA. Dpto. de Diseño y Fabricación, Catedrático. Calle María de Luna, 4 – 50018 Zaragoza (España).

2 INEGI. Dpto. de Materiales Compuestos y Estructuras. Campus da FEUP. R. Dr. Roberto Frías, 400, 4200-465 Porto (Portugal).

ABSTRACT:

Triply periodic minimal surface structures (TPMSs) can be used as a substitute for polymeric foams in applications where is necessary to absorb a large amount of energy with high structural deformation. Diamond TPMS offers higher energy absorption per unit weight. This structure is based on the Ashby-Gibson material model that establishes the main mechanical material properties as functions of the relative density and material properties. However, since TPMSs are used in dynamic applications, it is essential to analyse them under dynamic loads. In this study, we investigate the influence of the strain rate on the Ashby-Gibson parameters of sheet diamond

Keywords: Triple periodic minimal surface; strain rate; additive manufacturing; diamond; Ashby-Gibson

1. INTRODUCTION

Polymeric foams are extensively used in the packaging and automotive industries as internal liners in most types of helmets, side impact protection systems, seat cushions, envelopes for goods, bumper systems, etc. This is due to their high energy absorption per unit weight and high deformation in the process.

In addition, it is possible to tailor the mechanical properties of foams by controlling the expansion during the foaming process. The relationship between the density and the mechanical properties of these foams has been well-studied [1]. However, the manufacturing process of polymeric foams only yields constant density foams. Recent studies have revealed that, due to the differences in the stiffness of the elements that polymeric foams protect (i.e. in the case of a helmet, the human skull has different stiffness depending on the zone [2] and there are parts of the brain more sensitive to damages during impacts [3]), final products should have different properties depending on the zone that protects.

Recent advances in AM possibilities to create mono-block structures with different properties depending of the zone of piece and their structural requirements. Thus, it is possible to develop helmets with different stiffness in different zones of the brain to be protected [4].

One of the most promising AM structures are TPMS structures, also known as lattice structures, which are intricate periodic forms generated by repetition of cells. This cell is defined by a mathematical function that generates a surface with a minimum surface area, and as a result, maximizes the mechanical properties of the structure; hence, TPMS realizes high efficiency energy absorption per unit weight [5], and the properties also can be tailored. Additionally, there are several types of available materials for AM and thus, higher customization can be expected.

Among the different types of TPMS structures, Lidinoid, diamond, gyroid, Schwarz-P (primitive), Neovious, and split-P offer higher specific mechanical properties [6]. Comparative studies of these structures [7,8] have revealed that the diamond structure is ideal due to high energy absorption capability in the plateau zone per unit weigh, densification with a high strain, and stable stress levels in the plateau zone without "waves". Thus, we focus the diamond structure in this study.

Ashby and Gibson [9] analysed the stress-strain curves of different polymeric foams under quasi-static compression, and showed that these materials exhibit a characteristic curve. Additionally, these curves and the main mechanical properties are related to the density[10]. Recent studies have confirmed these behaviours in lattice structures [11,12] and cork products [13] as well.

The Ashby-Gibson model splits the stress-strain curve in three well-defined zones (see Fig. 1 of the supplementary material). The first zone is called the linear zone, where materials have an elastic and linear behaviour that defines the elastic Young's modulus (E_c) of the foam/lattice structure. In addition, in this zone, the walls of the cells of the foam or of the TPMS suffer elastic deformation without any permanent damage. After a certain point (defined when the actual curve deviates more than 0.2% from the elastic curve), cells of the foams and walls [14] of the TPMS begin to collapse or crush, and the material cannot recover its initial shape. Then, cells of foams and walls of TPMS structures collapse progressively with approximately similar levels of stress. As a result, the stress-strain curve exhibits a zone with approximately constant level of stress. In some cases, an initial peak appears [15], and in some TPMS structures,

Publicaciones DYNA SL -- c) Mazarredo nº 69 - 2º -- 48009-BILBAO (SPAIN)
Tel +34 944 237 566 – www.revistadyna.com - email: dyna@revistadyna.com

ISSN: 0012-7361 eISSN: 1989-1490 / DYNA Vol.98 n.5 DOI: https://doi.org/10.6036/10721

Pag. 1 / 11

some "waves" associated with the collapse of a layer appear. This zone is the plateau zone, where the average value of the stress defines the plateau Young's modulus (E_p). There is a point at which all the internal cells of the foam or TPMS collapse completely, and there is no air trapped inside the structure. At this point, the material densifies, and exhibits the same behaviour as the non-foamed material or of the original material in case of TPMS. As a result, the stress increases rapidly. This densification zone and transition point are denoted by $\varepsilon_{c,d}$ and $\sigma_{c,d}$, respectively, and is obtained in the intersection between the line defined by the plateau Young's modulus and bulk modulus of the solid material.

Additionally, the Ashby –Gibson model establishes a relationship between the properties of solid materials (elastic modulus E_s and yield stress σ_{ys}) and obtained lattice structures. Different equations are defined for closed cell and for open cell foams. In the case of lattice structures, this structures are equivalent to an open cell foam, because there is no fluid trapped inside. Additionally, Ashby-Gibson established different models for elastomeric foams (Eq. 1, Eq. 2, Eq. 3, and Eq. 6), elastic-plastic foams (Eq. 1, Eq. 4, Eq. 5, and Eq. 6), and elastic-brittle foams (Eq. 1, Eq. 6, and Eq. 7). The failure mechanism in the plateau zone changes totally. In elastomeric materials, an elastic buckling occurs due to the formation of plastic hinges and via brittle crushing in elastic-brittle foams. Eq. 2 and Eq. 3 differs due to the fact that the latter takes into consideration a correction due to the cell corners of cells in foams with a high ρ^* (> 0.3), which has the effect of making the foam slightly stronger. The same occurs in Eq. 4 and Eq. 5.

$$\frac{E_{c,foam/latt}}{E_S} = C_1 \cdot \left(\frac{\rho_{foam/latt}}{\rho_{C,solid}}\right)^m = C_1 \cdot \rho^{*m} \quad (1)$$

$$\frac{\sigma_{c,e,foam/latt}}{E_S} = C_3 \cdot \left(\frac{\rho_{foam/latt}}{\rho_{C,solid}}\right)^p = C_3 \cdot \rho^{*p} \qquad (2)$$

$$\frac{\sigma_{c,e,foam/latt}}{E_S} = C_3 \cdot \left(\frac{\rho_{foam/latt}}{\rho_{C,solid}}\right)^p \cdot \left[1 + \left(\frac{\rho_{foam/latt}}{\rho_{C,solid}}\right)^{1/2}\right]^2 = C_3 \cdot \rho^{*p} \cdot \left(1 + \rho^{*1/2}\right)^2 \qquad (3)$$

$$\frac{\sigma_{pl,foam/latt}}{\sigma_{ys}} = C_2 \cdot \left(\frac{\rho_{foam/latt}}{\rho_{C,solid}}\right)^n = C_2 \cdot \rho^{*n} \quad (4)$$

$$\frac{\sigma_{pl,foam/latt}}{\sigma_{ys}} = C_2 \cdot \left(\frac{\rho_{foam/latt}}{\rho_{C,solid}}\right)^n \cdot \left[1 + \left(\frac{\rho_{foam/latt}}{\rho_{C,solid}}\right)^{1/2}\right] = C_2 \cdot \rho^{*n} \cdot \left(1 + \rho^{*1/2}\right) \qquad (5)$$

$$\varepsilon_{c,p} = 1 - 1.4 \cdot \left(\frac{\rho_{foam/latt}}{\rho_{C,solid}}\right) = 1 - 1.4 \cdot \rho^* \quad (6)$$

$$\frac{\sigma^*_{cr,foam/latt}}{\sigma_{fs}} = C_4 \cdot \left(\frac{\rho_{foam/latt}}{\rho_{C,solid}}\right)^q = C_4 \cdot \rho^{*q} \qquad (7)$$

Here, C_i, n, m, p, and q are experimental variables. Analysis of the stress-strain curves of these structures (see. Fig. 1) are closed to an elastic-plastic Ashby-Gibson model. However, for the lowest volume fraction, the curve approximates an elastic-brittle model. Analysis of the failure mechanisms (Fig. 2 of the supplementary material) shows continuous shearing bands, generally of 45°, owing to crushed diagonal layers. Then, bending failure occurs, as reported previously [16].

Publicaciones DYNA SL -- c) Mazarredo nº 69 - 2º -- 48009-BILBAO (SPAIN)
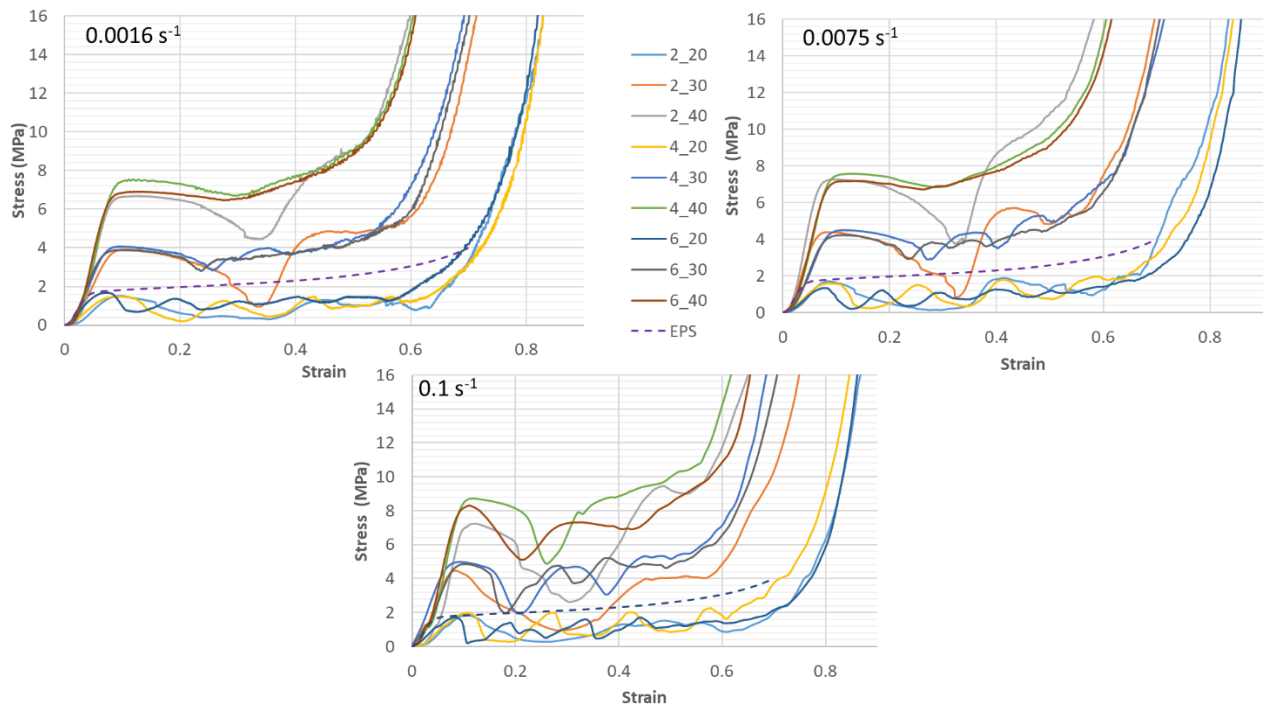Tel +34 944 237 566 – www.revistadyna.com - email: dyna@revistadyna.com

Pag. 2 / 11

Fig. 1. Stress-strain curves for analysed specimens under different strain rates.

In the case of elastic-plastic behaviour, Gibson-Ashby [9] indicated that C_1 is generally between 0.1 and 1, C_2 between 0.1 and 4, n and m depend on if the structure exhibits a bending-dominated collapse (n = 2 and m = 1.5) or stretch-dominated collapse (n = m = 1).

Moreover, Gibson- Ashby identified different collapse mechanisms in elastic-plastic materials. On the one hand, in stretch-dominated structures, there is an initial peak of the stress-strain curve after the elastic zone, followed by a post-yield softening where the levels of stress decreases. On the other hand, in bending-dominated structures, no local peak is observed in the onset. Fig. 2 shows that there is no initial peak, which confirms a bending dominated structure.

Although several studies have determined the Ashby-Gibson coefficient in lattice strut structures [17,18], sheet TPMS structures have not been investigated in detail [19–26] (see Table 1 of the supplementary material), and the influence of the strain rate has not been considered. Additionally, metal alloys (Ti₆Al₄V) have been studied, and there is only one papers of the state of the art that has studied a similar materials (ABS) but for a gyroid structure. In this case [24], regression has been used to obtain an elastic modulus C_1 of 0.23, an n of 1.14 (R2 96.5%), C_2 of 0.93, and a m of 1.97 (R2 95.5 %). Some studies have focused on the influence of the strain rate in other materials. Kang et al. [27] studied aluminium foams under three different strain rates (quasi-static, 650 s⁻¹ and 1600 s⁻¹), and observed that the parameters of the Ashby-Gibson model change depending on the strain rate. Similarly, Mae et al. [28] studied polypropylene foam under five different strain rates (0.3, 1, 10, 50, and 100 s⁻¹) and obtained similar results. Jain et al. [29] studied austenitic stainless steel foam under three different strain rates (0.1, 0.01, and 0.001 s⁻¹), and concluded that with a high R2, the higher the strain rate, the higher the values of C_1 and C_2 with the same n and m. Duan et al. [30] studied additive manufactured PLA Kelvin cells structures under five different strain rates (0.001, 0.01, 500, 1000, and 2000 s⁻¹), and observed that the Ashby-Gibson parameters after regression were different, and there was no clear relationship between the strain rate and the different parameters. The Ashby-Gibson model indicated that the strain rate influences the material behaviour of the constitutive materials of foam or lattice structures, but does not modify the experimental variables. Thus, only the modification of the properties of the constitutive materials need to be considered.

2.- MATERIALS AND METHODS

In this study, we investigate acrylonitrile styrene acrylate (ASA) with the commercial name Z-ASA Pro by Zortrax. All specimens were printed using a fused filament fabrication (FFF) Lion 2X 3D printer with a 0.4-mm nozzle and a layer height of 0.19 mm. Precisely, we investigate diamond structures that are defined as follows [31]:

$$F(x, y, z) = \sin\left(\frac{2\pi x}{a}\right)\sin\left(\frac{2\pi y}{a}\right)\sin\left(\frac{2\pi z}{a}\right) + \sin\left(\frac{2\pi x}{a}\right)\cos\left(\frac{2\pi y}{a}\right)\cos\left(\frac{2\pi z}{a}\right) + \cos\left(\frac{2\pi x}{a}\right)\sin\left(\frac{2\pi y}{a}\right)\cos\left(\frac{2\pi z}{a}\right) +$$
$$\cos\left(\frac{2\pi x}{a}\right)\cos\left(\frac{2\pi y}{a}\right)\sin\left(\frac{2\pi z}{a}\right) - t \qquad (8)$$

where x, y, and z are the coordinates, t is a constant adjusted for a desired volume fraction/wall thickness, and a is the cell size.

TPMS specimens were generated using N-Topology software using an implicit method that uses the volume fraction (ρ^*) instead of the thickness (t). The use of ρ^*, i.e., the relation of the density of the TPMS specimen (ρ_{latt}) and the density of the solid material (ρ_{solid}), is more common than the period in TPMS. However, there is a closed relationship between these parameters, given by:

$$\rho^* = \left(\frac{Volume_{struct}}{Volume_{solid}}\right) = \left(1 - \frac{\rho_{latt}}{\rho_{solid}}\right) \qquad (9)$$

It is worth noting that we do not focus on the influence of the strain rate in the Ashby-Gibson parameters, but the influence of the main parameters of the diamond structure ρ^* and a. Hence, we studied three different volume fractions and three different cell sizes (see Fig. 2), and three strain rates (0.0016, 0.0075, and 0.1 s^{-1}). ρ^* and a have been selected as functions of the maximum load capability of the uniaxial test machine, 3D printer's maximum resolution, and specimen dimensions (40 mm) comprising 6, 4, and 2 cells. The specimens have been named as X_YY, where X is the number of cells and YY is the volume fraction. It must be highlighted that in the case of low number of cells, some o edges effects could appear. The strain rates have been selected due to the maximum velocity of the uniaxial test machine.
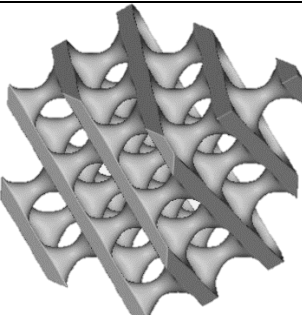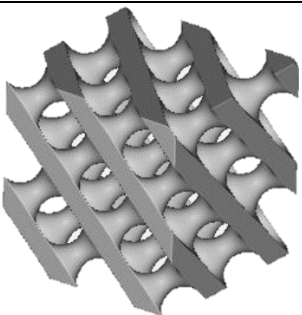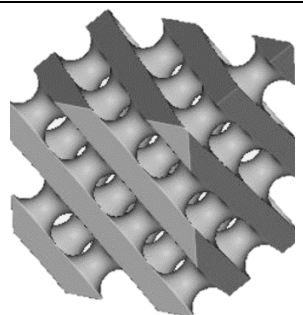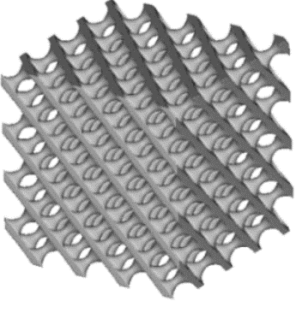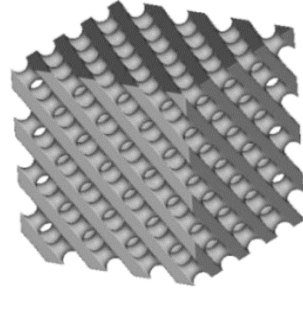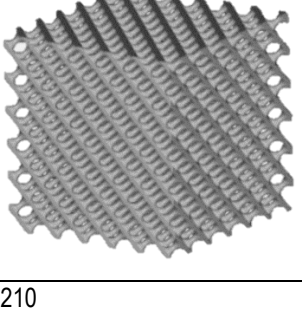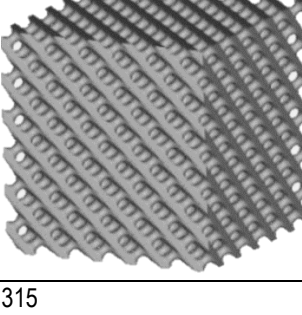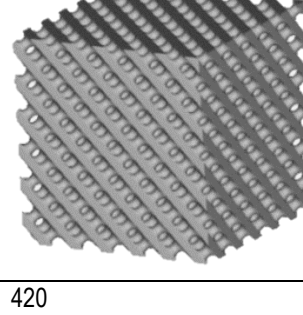
ρ^* vs. t	20%	30%	40%
6.6 mm			
10 mm			
20 mm			
Density. kg/m³	210	315	420

Fig. 2. N-Topology CAD models of the different specimens.

TPMS cubic specimens were studied under compression tests to obtain the mechanical properties of the structures. Moreover, full solid bone specimens were studied under traction tests to obtain material properties used to determine the Ashby-Gibson parameters (E_s and σ_{ys}).

There is no standard test for plastic TPMS structures. Due to the similarity of the main mechanical properties and stress-strain curves with cellular foams, the specific standards for these materials can be [32] the ASTM 3574, the ISO 844 or the ASTM. The main difference between these standards is the dimension of the specimen. The other aspects of the standards are similar. Due to the 3D printing machine resolution, maximum load capability of 100 kN of the INSTRON, and range of thickness and TPMS cell dimensions, we decided to use the ASTM D1621 standard, i.e., a 40 x 40 x 40 mm^3 prism specimen.

To determine the properties under traction loads in the case of the solid bone specimen, the ASTM D638 is the most common testing standard. All specimens were studied under quasi-static and dynamic compression loads using an 8032 INSTRON universal test machine with a maximum load capability of 100 kN. To measure the force and determine the stress using the transversal area of the specimen in the case of the TPMS specimens, a 100 kN load cell was used, and in the case of bone specimens with much lower transversal area, a 10 kN load cell was used to reduce the load cell error.

In terms of the strain rate, all mentioned regulations are specific for quasi-static load cases and specify the same movement condition (there are not any regulation for dynamic load cases). The rate of crosshead displacement must be equal to 10 % of the sample thickness per minute. Thus, for the TPMS prism, the velocity must be 4 mm/min, which imply a strain rate of 0.0016 s^{-1}. In the case of the bone specimens, the extensometer was sued to control the strain rate, which was fixed at 0.0016 s^{-1}. In the case of the dynamic test, the maximum velocity of the INSTRON test machine (4 mm/s) limited the maximum strain rate, and thus, it was fixed at 0.1 s^{-1}. We also selected an intermediate strain rate of 0.0075 s^{-1} (0.3 mm/s). In the case of the bone test, the extensometer was used to control the strain rate. It must be also be noted that for FFF printed structures, the print direction can affect the results [33], and thus, all the specimens were tested in the print direction

The results of the TPMS test were processed to obtain the stress-strain curves (see Fig. 1), using which the main mechanical properties (see Table 1) were evaluated in detail in previous articles [34,35]. Additionally, the stress-strain curves have been obtained, using which the main mechanical properties (see Table 2 of the supplementary material and Fig. 3 of the supplementary material) for the solid material were determined to be used in Eqs. 1 to 7. It can be observed that the higher the strain rate, the higher the elastic Young's modulus (E_s), ultimate strength (σ_{ys}), and elongation at maximum tensile stress (ε_{ys}), in agreement with previously reported results for other materials [36,37]

0.0016 s^{-1}								0.0075 s^{-1}					
Cells/ρ*		E_c	$\sigma_{c,e}$	$\sigma_{c,p}$	$\sigma_{c,d}$	$\varepsilon_{c,e}$	$\varepsilon_{c,p}$	E_c	$\sigma_{c,e}$	$\sigma_{c,p}$	$\sigma_{c,d}$	$\varepsilon_{c,e}$	$\varepsilon_{c,p}$
		MPa				%		MPa				%	
2	20%	26.8	1.4	1.1	0.9	5.2	63.4	34.5	1.6	1.0	2.0	4.6	67.3
	30%	59.4	3.7	2.6	5.1	6.2	59.3	91.0	4.0	3.0	5.2	4.4	58.4
	40%	126.8	6.2	5.6	9.0	4.9	51.1	141.0	6.8	6.0	11.0	4.8	47.2
4	20%	25.1	1.4	1.1	1.4	5.6	61.7	27.6	1.5	1.0	1.8	5.4	63.4
	30%	72.8	3.8	3.3	4.8	5.2	53.2	72.0	4.1	3.8	5.2	5.7	51.2
	40%	132.0	6.5	7.0	9.0	4.9	51.3	121.0	6.8	7.2	10.0	5.6	49.9
6	20%	36.8	1.6	1.2	1.5	4.3	58.4	24.6	1.2	0.9	1.8	4.9	66.7
	30%	72.2	3.8	3.4	5.0	5.3	57.8	70.5	4.2	3.6	4.8	6.0	55.3
	40%	134.2	7.2	6.6	9.0	5.4	52.2	119.0	6.8	7.0	10.0	5.7	52.3

0.1 s^{-1}							
Cells/ρ*		E_c	$\sigma_{c,e}$	$\sigma_{c,p}$	$\sigma_{c,d}$	$\varepsilon_{c,e}$	$\varepsilon_{c,p}$
		MPa				%	
2 cells	20%	23.5	1.7	1.0	1.7	7.2	62.6
	30%	69.0	4.2	3.0	4.0	6.1	60.2
	40%	140.0	6.9	6.0	9.0	4.9	53.3
	20%	23.3	1.9	1.1	1.5	8.2	61.3

Publicaciones DYNA SL -- c) Mazarredo nº 69 - 2º -- 48009-BILBAO (SPAIN)
Tel +34 944 237 566 – www.revistadyna.com - email: dyna@revistadyna.com

Pag. 5 / 11

ISSN: 0012-7361 eISSN: 1989-1490 / DYNA Vol.98 n.5 DOI: https://doi.org/10.6036/10721

4 cells	30%	66.1	4.6	3.6	5.4	7.0	50.2
	40%	112.0	8.0	7.2	10.2	7.1	57.8
6 cells	20%	22.7	1.8	1.0	1.9	7.9	63.3
	30%	63.3	4.6	3.6	5.0	7.3	57.2
	40%	122.0	7.8	7.0	10.0	6.4	56.0

Table 1. Main mechanical properties of the tested specimens

3. - RESULTS AND DISCUSSION

Fig. 1 shows that all the specimens follow the Ashby-Gibson material model, and that the higher the relative density, the higher the stress values, and the lower the strain in the densification point. In addition, it can be observed that the lower the number of cells, the higher the instability, which is also reflected in a depth valley in the plateau zone associated with the collapse of one layer of the specimen. It can be observed that for lower strain rates (0.0016 s^{-1} and 0.0075 s^{-1}) and higher volume fractions (20 and 30%), there is no initial peak. Thus, it can be deduced that these are bending-dominated structures. In the case of 20% volume fraction and for the highest strain rates, an initial peak occurs, and then, a post-yield softening that could indicate a stretching-dominated structure is observed. However, new peaks also appear in the plateau zone, which indicates the instability of the structure. The analysis of the failure mechanism (Fig. 2 of the supplementary material) reveals that failure due to bending predominates in all cases.

It can also be observed that the higher strain rate, the higher the instability of the curves and a higher influence of the number of cells/period in the shape and values of the curve. Additionally, it the results for the 120 kg/m^3 EPS show that the stress-strain curve is between the results for the diamond structure with a volume fraction of 20% (210 kg/m^3) and 30% (315 kg/m^3). It must also be noted that EPS does not suffer from instability when the strain rate increases, and has a significantly lower density.

Using Eqs. 1, 4 and 5, the relationship between the logarithm of the volume fraction vs. the logarithm of the elasticity (Fig. 6) and stiffness are plotted without taking into consideration a correction due to the cell corners (Fig. 4 of the supplementary material), and by considering the correction (Fig. 5 of the supplementary material). With a high R^2, there is a linear relationship, and it can be deduced that these equations can be also used to determine the final properties. Then, C_1, C_2, n, and m can be obtained (Table 2) as varying functions of the strain rate, as reported previously for foams [27,28]. A relationship depending on the number of cells and a global relationship for all cases with high R^2, but slightly lower than previously, have also been obtained.

Fig. 3. logarithm of the volume fraction vs. the logarithm of the elasticity

Publicaciones DYNA SL -- c) Mazarredo nº 69 - 2º -- 48009-BILBAO (SPAIN)
Tel +34 944 237 566 – www.revistadyna.com - email: dyna@revistadyna.com

Pag. 6 / 11

ISSN: 0012-7361 eISSN: 1989-1490 / DYNA Vol.98 n.5 DOI: https://doi.org/10.6036/10721

	2 cells						4 cells					
	Stiffness		Corrected		Elastic		Stiffness		Corrected		Elastic	
strain rate	m	C_2	m	C_2	n	C_1	m	C_2	m	C_2	n	C_1
0.00167 s^{-1}	1.18	2.33	0.62	2.16	0.48	2.22	2.10	2.67	1.10	2.50	0.65	2.41
0.0075 s^{-1}	1.29	2.59	0.67	2.42	0.38	2.05	2.10	2.88	1.10	2.70	0.35	2.15
0.1 s^{-1}	1.12	2.59	0.59	2.42	0.56	2.58	1.53	2.72	0.80	2.55	0.36	2.29
	6 cells						All cells					
	Stiffness		Corrected		Elastic		Stiffness		Corrected		Elastic	
strain rate	m	C_2	m	C_2	n	C_1	m	C_2	m	C_2	n	C_1
0.00167 s^{-1}	1.66	2.47	0.87	2.29	0.37	1.85	1.60	2.49	0.84	2.32	0.49	2.16
0.0075 s^{-1}	1.32	2.59	1.19	2.82	0.38	2.03	1.83	2.82	0.96	2.65	0.37	2.17
0.1 s^{-1}	1.68	2.83	0.88	2.66	0.43	2.43	1.42	2.72	0.74	2.54	0.44	2.43

Table 2. Ashby-Gibson parameters for the studied specimens

Table 3 of the supplementary material shows the error obtained using Eqs. 1, 4, and 5, and the Ashby-Gibson parameters obtained using a regression. It can be seen that Eq. 1 can predict the E^* with a low error. Similarly, Eqs. 4 and 5 can also predict the average stress level in the plateau zone with a low error for the lowest and highest strain rates. In the case of the 0.0075 s^{-1} rate, the error is higher than 10%. It must also be pointed that both equations have a similar accuracy, and thus, Eq. 4 would be more adequate since it is simpler. Moreover, in this case, different Ashby-Gibson parameters have been obtained for each number of cells/periods and for each strain rate. We also determined Ashby-Gibson parameters independently of the number of cells by considering the strain rate. The results in Table 3 of the supplementary material show that high errors occur in this case, and thus, it cannot be used to determine mechanical properties.

Additionally, we used Eq. 6 to determine $\varepsilon_{c,d}$ (see Table 1), but the results show a high error, and thus, this equation cannot be used.

Fig. 4, Fig. 6 of the supplementary material, and Fig. 7 of the supplementary material show plots of the numerical results obtained using the Ashby-Gibson model with Eqs. 1, 4, and 5, respectively. It can be observed that there is no clear relationship between the number of cells in the values for the E^* and σ_{latt}.

Publicaciones DYNA SL -- c) Mazarredo nº 69 - 2º -- 48009-BILBAO (SPAIN)
Tel +34 944 237 566 – www.revistadyna.com - email: dyna@revistadyna.com

Pag. 7 / 11

ISSN: 0012-7361 eISSN: 1989-1490 / DYNA Vol.98 n.5 DOI: https://doi.org/10.6036/10721
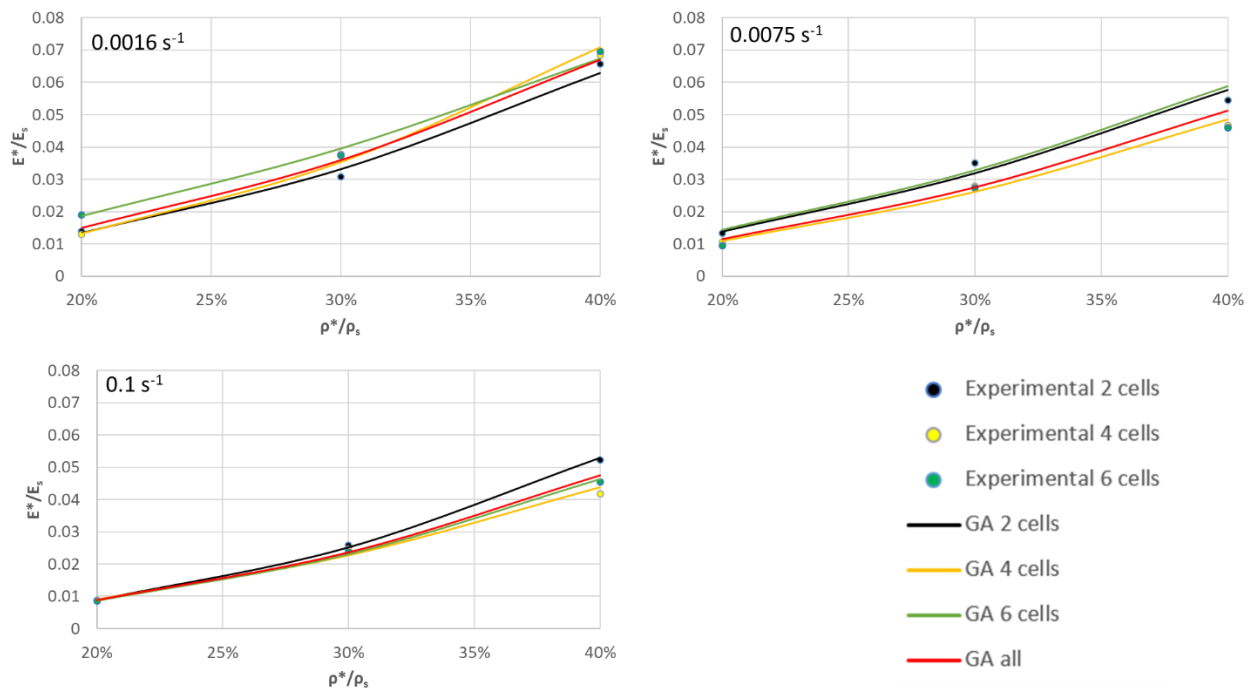
Fig. 4. Numerical results for the elastic Young's modulus. Experimental and analytical with eq. 1.

Similarly, the analysis of the relationship of the of the Ashby-Gibson parameters with the strain rate and number of cells (Fig. 5) shows that there is no clear tendency, and it cannot be estimated like previously reported results for PLA foams [30]. Thus, the parameters must be experimentally established for each strain rate.
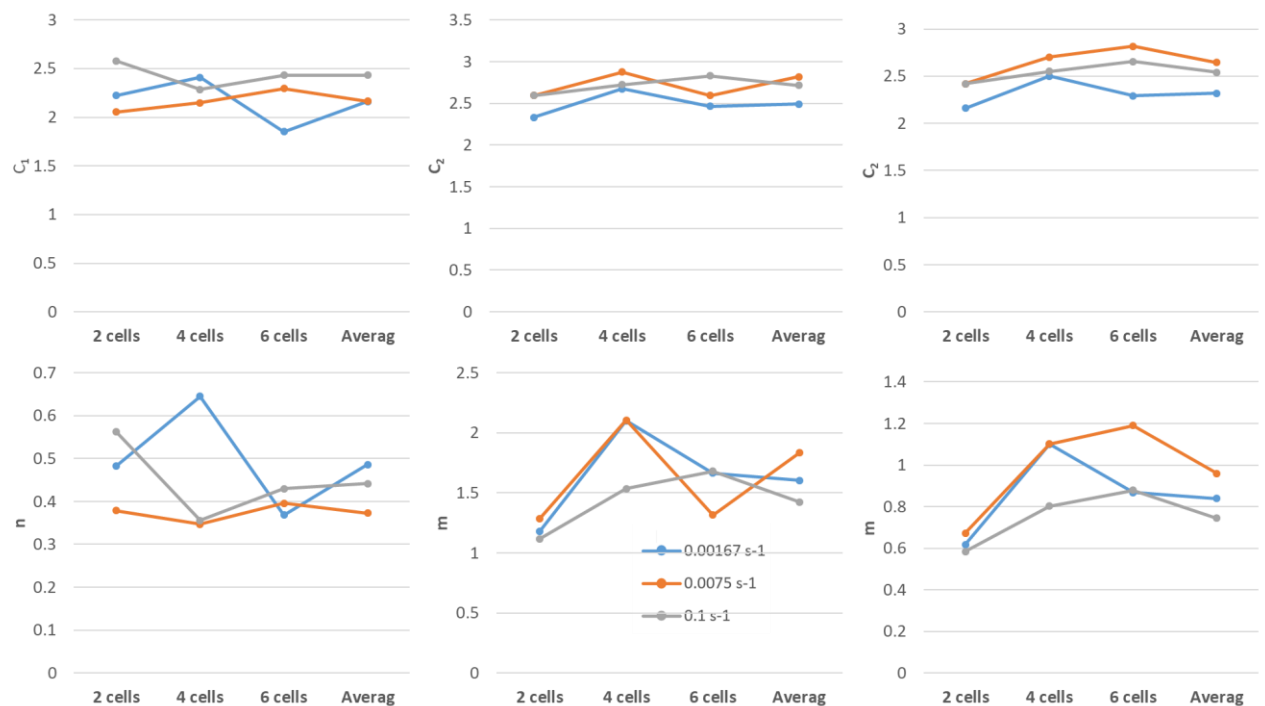

Fig. 5. Comparative analysis of the obtained parameters in function of the number of cells and the strain rate.

Publicaciones DYNA SL -- c) Mazarredo nº 69 - 2º -- 48009-BILBAO (SPAIN)
Tel +34 944 237 566 – www.revistadyna.com - email: dyna@revistadyna.com

Pag. 8 / 11

ISSN: 0012-7361 eISSN: 1989-1490 / DYNA Vol.98 n.5 DOI: https://doi.org/10.6036/10721

It was observed that the C_1 and C_2 (for Eqs. 4 and 5) parameters are between 2 and 3, n is between 0.3 and 0.7, m (of Eq. 4) is between 1.1 and 2.1, and m (of Eq.) is between 0.6 and 1.2. Thus, while C_1 and C_2 the are inside the ranges proposed by Gibson and Ashby [9], n and m are not similar to the proposed ones for bending-dominated collapse. The values also differ from other recent results [19–26] (see Table 1 of the supplementary material), but the TPMS analysed here and the materials in these previous studies is different.

4. - CONCLUSIONS

Our results present valuable information about the behaviour of the PLA diamond TPMS and the influence of the strain rate and internal parameters on the Ashby-Gibson parameters generated by FFF AM.

The main conclusions drawn from this study are as follows: The investigated structure follows the Ashby-Gibson material model, and the higher the volume fraction, the higher the mechanical properties (stress levels, capability to absorb energy, etc.), but the lower the strain in the densification point for any strain rate. In addition, the cell size does not have significant influence on the mechanical properties for low and moderate strain rates, but in the case of a low number of cells, some abrupt drops appear in the plateau zone due this effect. It has been also observed that the higher the strain rate, the more unstable the material, and more differences appear in the behaviour due to the number of cells. Additionally, the maximum stress level in the elastic zone increases.

Furthermore, it is possible to obtain the Ashby-Gibson parameters of the curve with a high R^2, and the results show the experimental date adjust to this material model laws with a low error. However, there is no clear relationship between the strain rate and number of cells in these Ashby-Gibson parameters. It must be pointed that for average stress levels in the plateau zone, both models have the same accuracy with and without taking into consideration a correction due to the cell corners.

The Ashby-Gibson equation proposed to determine the strain in the densification point it is not sufficiently accurate. The analysis of the obtained Ashby-Gibson parameters has also reflected that there is no clear tendency in predicting the variation of the parameters as functions of the number of cells/periods and strain rate.

Moreover, the ASA diamond structure cannot substitute EPS, because it offers lower mechanical properties per unit weight. Additionally, EPS is more stable in the plateau zone. Consequently, other materials should also be studied, for instance carbon fibre reinforced materials and polyamides.

Finally, it has been observed that main failure mechanism in diamond structures is due to bending, and generally, this failure first appears along a diagonal of the structure, and then, subsequently, it appears in adjacent ones. Consequently, the initial peak in the densification zone does not appear in the stress-strain curve.

To summarize, the diamond structure follows the Ashby-Gibson model, and it is possible to obtain the Ashby-Gibson parameters using a regression. However, they cannot be predicted as functions of the number of cells and/or the strain rate, and thus, must be determined experimentally for each case. This is the main drawback of this model, because it is not possible to predict the main mechanical properties with a low number of experimental tests due to the fact that the change with the strain rate and number of cells cannot be determined.

REFERENCES

[1] C. Ling, J. Ivens, P. Cardiff, M.D. Gilchrist, Deformation response of EPS foam under combined compression-shear loading. Part I: Experimental design and quasi-static tests, International Journal of Mechanical Sciences. 144 (2018) 480–489. https://doi.org/10.1016/j.ijmecsci.2018.06.014.

[2] A.M. Loyd, R.W. Nightingale, J.F. Luck, Y. Song, L. Fronheiser, H. Cutcliffe, B.S. Myers, C.R. Dale Bass, The compressive stiffness of human pediatric heads, Journal of Biomechanics. 48 (2015) 3766–3775. https://doi.org/10.1016/j.jbiomech.2015.08.024.

[3] J. Michio Clark, A. Post, T. Blaine Hoshizaki, M.D. Gilchrist, Distribution of Brain Strain in the Cerebrum for Laboratory Impacts to Ice Hockey Goaltender Masks, Journal of Biomechanical Engineering. 140 (2018) 121007. https://doi.org/10.1115/1.4040605.

[4] S.F. Khosroshahi, H. Duckworth, U. Galvanetto, M. Ghajari, The effects of topology and relative density of lattice liners on traumatic brain injury mitigation, Journal of Biomechanics. 97 (2019) 109376. https://doi.org/10.1016/j.jbiomech.2019.109376.

[5] L. Zhang, S. Feih, S. Daynes, S. Chang, M.Y. Wang, J. Wei, W.F. Lu, Energy absorption characteristics of metallic triply periodic minimal surface sheet structures under compressive loading, Additive Manufacturing. 23 (2018) 505–515. https://doi.org/10.1016/j.addma.2018.08.007.

[6] A. Panesar, M. Abdi, D. Hickman, I. Ashcroft, Strategies for functionally graded lattice structures derived using topology optimisation for Additive Manufacturing, Additive Manufacturing. 19 (2018) 81–94. https://doi.org/10.1016/j.addma.2017.11.008.

[7] R. Miralbes, D. Ranz, F.J. Pascual, D. Zouzias, M. Maza, Characterization of additively manufactured triply periodic minimal surface structures under compressive loading, Mechanics of Advanced Materials and Structures. (2020) 1–15. https://doi.org/10.1080/15376494.2020.1842948.

[8] J. Podroužek, M. Marcon, K. Ninčević, R. Wan-Wendner, Bio-Inspired 3D Infill Patterns for Additive Manufacturing and Structural Applications, Materials. 12 (2019) 499. https://doi.org/10.3390/ma12030499.

[9] L.J. Gibson, M.F. Ashby, Cellular Solids: Structure and Properties, 2nd ed., Cambridge University Press, 1997. https://doi.org/10.1017/CBO9781139878326.

[10] S. Doroudiani, M.T. Kortschot, Polystyrene foams. III. Structure-tensile properties relationships, J. Appl. Polym. Sci. 90 (2003) 1427–1434. https://doi.org/10.1002/app.12806.

[11] Z. Alomar, F. Concli, A Review of the Selective Laser Melting Lattice Structures and Their Numerical Models, Adv. Eng. Mater. 22 (2020) 2000611. https://doi.org/10.1002/adem.202000611.

[12] S. Higuera, R. Miralbes, D. Ranz, Mechanical properties and energy–absorption capabilities of thermoplastic sheet gyroid structures, Mechanics of Advanced Materials and Structures. (2021) 1–15. https://doi.org/10.1080/15376494.2021.1919803.

[13] R. Miralbes, D. Ranz, J. Ivens, J.A. Gomez, Characterization of cork and cork agglomerates under compressive loads by means of energy absorption diagrams, Eur. J. Wood Prod. (2020). https://doi.org/10.1007/s00107-020-01625-7.

[14] I. Maskery, L. Sturm, A.O. Aremu, A. Panesar, C.B. Williams, C.J. Tuck, R.D. Wildman, I.A. Ashcroft, R.J.M. Hague, Insights into the mechanical properties of several triply periodic minimal surface lattice structures made by polymer additive manufacturing, Polymer. 152 (2018) 62–71. https://doi.org/10.1016/j.polymer.2017.11.049.

[15] K.Y.G. McCullough, N.A. Fleck, M.F. Ashby, Uniaxial stress–strain behaviour of aluminium alloy foams, Acta Materialia. 47 (1999) 2323–2330. https://doi.org/10.1016/S1359-6454(99)00128-7.

[16] X.-Y. Zhang, G. Fang, J. Zhou, Additively Manufactured Scaffolds for Bone Tissue Engineering and the Prediction of their Mechanical Behavior: A Review, Materials. 10 (2017) 50. https://doi.org/10.3390/ma10010050.

[17] C. Tian, X. Li, H. Li, G. Guo, L. Wang, Y. Rong, The effect of porosity on the mechanical property of metal-bonded diamond grinding wheel fabricated by selective laser melting (SLM), Materials Science and Engineering: A. 743 (2019) 697–706. https://doi.org/10.1016/j.msea.2018.11.138.

[18] D.S.J. Al-Saedi, S.H. Masood, M. Faizan-Ur-Rab, A. Alomarah, P. Ponnusamy, Mechanical properties and energy absorption capability of functionally graded F2BCC lattice fabricated by SLM, Materials & Design. 144 (2018) 32–44. https://doi.org/10.1016/j.matdes.2018.01.059.

[19] T. Maconachie, M. Leary, B. Lozanovski, X. Zhang, M. Qian, O. Faruque, M. Brandt, SLM lattice structures: Properties, performance, applications and challenges, Materials & Design. 183 (2019) 108137. https://doi.org/10.1016/j.matdes.2019.108137.

[20] S.M. Ahmadi, G. Campoli, S. Amin Yavari, B. Sajadi, R. Wauthle, J. Schrooten, H. Weinans, A.A. Zadpoor, Mechanical behavior of regular open-cell porous biomaterials made of diamond lattice unit cells, Journal of the Mechanical Behavior of Biomedical Materials. 34 (2014) 106–115. https://doi.org/10.1016/j.jmbbm.2014.02.003.

[21] C. Yan, L. Hao, A. Hussein, P. Young, Ti–6Al–4V triply periodic minimal surface structures for bone implants fabricated via selective laser melting, Journal of the Mechanical Behavior of Biomedical Materials. 51 (2015) 61–73. https://doi.org/10.1016/j.jmbbm.2015.06.024.

[22] M.R. Bach, V.B. Chalivendra, C. Alves, E. Depina, Mechanical characterization of natural biodegradable sandwich materials, Jnl of Sandwich Structures & Materials. 19 (2017) 482–496. https://doi.org/10.1177/1099636215622143.

[23] S. Ahmadi, S. Yavari, R. Wauthle, B. Pouran, J. Schrooten, H. Weinans, A. Zadpoor, Additively Manufactured Open-Cell Porous Biomaterials Made from Six Different Space-Filling Unit Cells: The Mechanical and Morphological Properties, Materials. 8 (2015) 1871–1896. https://doi.org/10.3390/ma8041871.

[24] T. Maconachie, R. Tino, B. Lozanovski, M. Watson, A. Jones, C. Pandelidi, A. Alghamdi, A. Almalki, D. Downing, M. Brandt, M. Leary, The compressive behaviour of ABS gyroid lattice structures manufactured by fused deposition modelling, Int J Adv Manuf Technol. 107 (2020) 4449–4467. https://doi.org/10.1007/s00170-020-05239-4.

[25] S.-Y. Park, K.-S. Kim, B. AlMangour, D. Grzesiak, K.-A. Lee, Effect of unit cell topology on the tensile loading responses of additive manufactured CoCrMo triply periodic minimal surface sheet lattices, Materials & Design. 206 (2021) 109778. https://doi.org/10.1016/j.matdes.2021.109778.

[26] C. Han, Y. Li, Q. Wang, S. Wen, Q. Wei, C. Yan, L. Hao, J. Liu, Y. Shi, Continuous functionally graded porous titanium scaffolds manufactured by selective laser melting for bone implants, Journal of the Mechanical Behavior of Biomedical Materials. 80 (2018) 119–127. https://doi.org/10.1016/j.jmbbm.2018.01.013.

[27] Y. Kang, J. Zhang, J. Tan, Compressive behavior of aluminum foams at low and high strain rates, J Cent. South Univ. Technol. 14 (2007) 301–305. https://doi.org/10.1007/s11771-007-0269-8.

[28] H. Mae, M. Omiya, K. Kishimoto, Effects of strain rate and density on tensile behavior of polypropylene syntactic foam with polymer microballoons, Materials Science and Engineering: A. 477 (2008) 168–178. https://doi.org/10.1016/j.msea.2007.05.028.

[29] H. Jain, D.P. Mondal, G. Gupta, R. Kumar, Effect of compressive strain rate on the deformation behaviour of austenitic stainless steel foam produced by space holder technique, Materials Chemistry and Physics. 259 (2021) 124010. https://doi.org/10.1016/j.matchemphys.2020.124010.

[30] Y. Duan, B. Du, X. Shi, B. Hou, Y. Li, Quasi-static and dynamic compressive properties and deformation mechanisms of 3D printed polymeric cellular structures with Kelvin cells, International Journal of Impact Engineering. 132 (2019) 103303. https://doi.org/10.1016/j.ijimpeng.2019.05.017.

[31] S. Hyde, ed., The Language of shape: the role of curvature in condensed matter--physics, chemistry, and biology, Elsevier, Amsterdam [Netherlands] ; New York, 1997.

[32] R. Miralbes, S. Higuera, D. Ranz, J.A. Gomez, Comparative analysis of mechanical properties and energy absorption capabilities of functionally graded and non-graded thermoplastic sheet gyroid structures, Mechanics of Advanced Materials and Structures. (2021) 1–14. https://doi.org/10.1080/15376494.2021.1949509.

[33] S. Raam Kumar, S. Sridhar, R. Venkatraman, M. Venkatesan, Polymer additive manufacturing of ASA structure: Influence of printing parameters on mechanical properties, Materials Today: Proceedings. 39 (2021) 1316–1319. https://doi.org/10.1016/j.matpr.2020.04.500.

[34] R. Miralbes, N. Santamaria, D. Ranz, J.A. Gomez, Mechanical properties of diamond lattice structures based on main parameters and strain rate, Mechanics of Advanced Materials and Structures. (2022) 1–13. https://doi.org/10.1080/15376494.2022.2081749.

[35] R. Miralbes, N. Santamaria, D. Ranz, J.A. Gómez, Study of the Anisotropy of Triple Periodic Minimal Surface Structures Generate by Additive Manufacturing, in: S. Gerbino, A. Lanzotti, M. Martorelli, R. Mirálbes Buil, C. Rizzi, L. Roucoules (Eds.), Advances on Mechanics, Design Engineering and Manufacturing IV, Springer International Publishing, Cham, 2023: pp. 905–913. https://doi.org/10.1007/978-3-031-15928-2_79.

[36] A. Vairis, M. Petousis, N. Vidakis, K. Savvakis, On the Strain Rate Sensitivity of Abs and Abs Plus Fused Deposition Modeling Parts, J. of Materi Eng and Perform. 25 (2016) 3558–3565. https://doi.org/10.1007/s11665-016-2198-x.

Publicaciones DYNA SL -- c) Mazarredo nº 69 - 2º -- 48009-BILBAO (SPAIN)
Tel +34 944 237 566 – www.revistadyna.com - email: dyna@revistadyna.com

Pag. 10 / 11

ISSN: 0012-7361 eISSN: 1989-1490 / DYNA Vol.98 n.5 DOI: https://doi.org/10.6036/10721

[37] K. Hibbert, G. Warner, C. Brown, O. Ajide, G. Owolabi, A. Azimi, The Effects of Build Parameters and Strain Rate on the Mechanical Properties of FDM 3D-Printed Acrylonitrile Butadiene Styrene, OJOPM. 09 (2019) 1–27. https://doi.org/10.4236/ojopm.2019.91001.

SUPPLEMENTARY MATERIAL

https://www.revistadyna.com/documentos/pdfs/_adic/10721-1_en.pdf